

Synthesis, Optical and Electrical Properties of ZnFe_2O_4 Nanocomposites

Regular Paper

G.S. Yashavanth Kumar¹, H.S. Bhojya Naik^{1,*}, A.S. Roy¹, K. N. Harish¹, R. Viswanath¹

¹ Department of Studies and Research in Industrial Chemistry, School of Chemical Sciences, Kuvempu University, India

² Department of Materials Science, Gulbarga University, Karnataka, India

* Corresponding author E-mail: hsb_naik@rediffmail.com

Received 15 Nov 2012; Accepted 20 Dec 2012

© 2013 Kumar et al.; licensee InTech. This is an open access article distributed under the terms of the Creative Commons Attribution License (<http://creativecommons.org/licenses/by/3.0>), which permits unrestricted use, distribution, and reproduction in any medium, provided the original work is properly cited.

Abstract ZnFe_2O_4 nanocomposites have been prepared by a simple co-precipitation method. The prepared samples were characterized by Scanning Electron Microscopy (SEM), Powder X-ray Diffraction (XRD), Energy Disperse X-ray Analysis (EDX), Transmission electron microscopy (TEM) and UV-visible absorption spectral techniques. Conductivity measurements show a transition from ferrimagnetism to paramagnetism. The enhancement in fluorescence spectra shows that there is an electronic transition to an exciting level. In UV-Vis spectra, the peak observed at 647nm indicates ZnFe_2O_4 nanocomposites are a photoactive compound. The above results suggest that these nanomaterials can be used in optoelectronic applications.

Keywords Optoelectronic, Fluorescence, Conductivity, Ferrite, Nanocomposite.

1. Introduction

The development of optical nanoparticles has resulted in major advantages in biological applications, such as imaging and sensing, since the 1990s [1-2]. These applications require monodisperse and photostable properties in nanoparticles, which are amenable to

further surface modification for the conjugation of fluorophores [3]. So far various approaches have been developed to synthesize magnetic fluorescent bi-functional nanocomposites [4]. For example, the use of magnetic Zn^{2+} , Co^{2+} and Mn^{2+} ions to partially substitute Cd^{2+} or Zn^{2+} ions in CdSe or ZnSe nanocrystals. Other research involved the preparation of $\text{Fe}_3\text{O}_4/\text{CdSe}$ and $\text{Fe}_2\text{O}_3/\text{CdSe}$ nanocomposites with magnetic properties [5-6]. The stability of ferrite nanocomposites is applicable in microwave devices because Zn and Ni ferrite have high resistivity, a high Curie temperature, chemical stability and good magnetic properties at high frequencies [7].

Recent research in this field has mainly focused on increasing the quantum yields of synthetic quantum dots (QDs), which can be diversely applied in biotechnology, sensors, superconductors etc. The substituted magnetic QD composites are expected to have more opportunities for technological application, especially in medical fields [8-10]. Kim et al. [11] reported the preparation of bi-functional magnetic-optical nanocrystals by growing a luminescent CdSe shell over metallic cobalt nanoparticles. Current investigations reveal that the ZnFe_2O_4 nanocomposites were active, due to their great sensitivity towards the photoelectronic properties.

2. Experiments

The $\text{ZnSO}_4 \cdot 7\text{H}_2\text{O}$, $\text{FeSO}_4 \cdot 7\text{H}_2\text{O}$, FeCl_3 and sodium hydroxide (NaOH) used were analytical grade and were used without further purification.

Synthesis of ZnFe_2O_4 nanocomposites was prepared by employing a co-precipitation method [12] by taking high-purity $\text{ZnSO}_4 \cdot 7\text{H}_2\text{O}$, $\text{FeSO}_4 \cdot 7\text{H}_2\text{O}$ and FeCl_3 as starting materials. The proper stoichiometry of the starting materials was weighed separately, followed by the addition of a suitable quantity of de-ionized water to make 0.5M solution, which was stirred for 1 hour to obtain a homogeneous solution. A 1M NaOH solution was added drop wise into the above solution at 333K with constant stirring until the precipitation was obtained. Further heating of the precipitate in its alkaline condition was continued at a soaking temperature of 373K for 6 hours in order to get the ZnFe_2O_4 nanocomposites. Finally, the obtained precipitate was washed with double distilled water repeatedly and dried at 333K for 12 hours. The obtained ferrites are deagglomerated by grinding using an agate mortar and pestle in acetone to obtain very fine particles. These particles were calcinated in a silica crucible at 673K for further crystallization [13].

3. Methods

The synthesized ZnFe_2O_4 nanocomposites were subjected to X-ray diffraction studies [using a Phillips X'pert diffractometer and a Cu K_α radiation source $\lambda = 0.154\text{nm}$] to determine the crystal phase composition. Elemental analysis was carried out by an energy dispersed X-ray analysis (EDAX) spectrum and surface morphology was studied by scanning electron microscopy (SEM: Hitachi S-4800). Transmission electron microscope (TEM) experiments were carried out on a JEOL JEM2010 transmission electron microscope operated at 200kV. The optical properties of this sample were investigated by using a UV-Visible absorption spectrophotometer (Shimadzu PC 1650 model) and fluorescence spectra taken from a spectrofluorophotometer (Shimadzu RF 5301 model).

The electrical conductivity measurements were conducted using a KEITHLEY source meter (Model – 4240). The powder nanocomposite samples were pressed uniaxially into a 2mm thick pellet with a diameter of 10mm by applying 120Mpa of pressure for 3 minutes. The pellets were sintered for thermal stability at 300K for 3 hours and silver paste was applied on both sides of the pellets for better contact with the electrode. The DC electrical conductivity measurements were carried out at a temperature between the range of 300-650K and electrical conductivity σ was calculated by the formula mentioned below (1).

$$\sigma = It/VA \quad (1)$$

where 'V' is the applied voltage, 'I' is the measured current, 'A' is the area of the pellet and 't' is thickness of the pellet. The Arrhenius equation, which relates the electrical conductivity and the temperature, is given by:

$$\sigma = \sigma_0 \exp \{-E_a/K_B T\} \quad (2)$$

Where E_a is the activation energy, K_B is Boltzmann constant and T is the temperature. The activation energy was calculated from an Arrhenius plot.

4. Results and discussion

Figure 1 illustrates XRD patterns of synthesized ZnFe_2O_4 nanocomposite powder after calcinations. From the curve all the observed diffraction peaks can be indexed to a cubic spinel phase with fcc structure magnetite according to JCPDS card No 82-1042. Six characteristic peaks marked by their Miller indices (220), (311), (400), (422), (511) and (440) with 100% intensity at $2\theta = 34.87^\circ$ correspond to the reflection plane (311). The average particle size was determined by Debye-Scherrer's formula, that is $20\text{ nm} \pm 5\text{ nm}$.

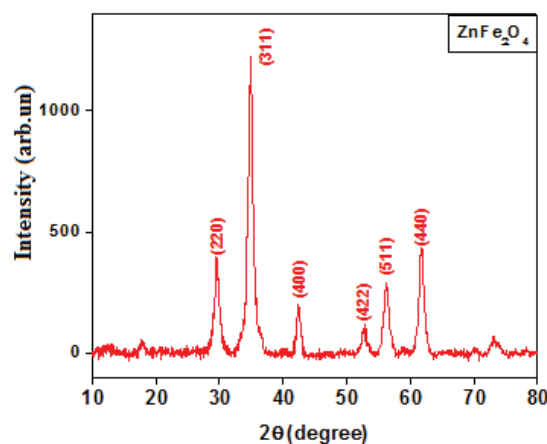


Figure 1. X-ray Diffraction pattern of ZnFe_2O_4 nanocomposites.

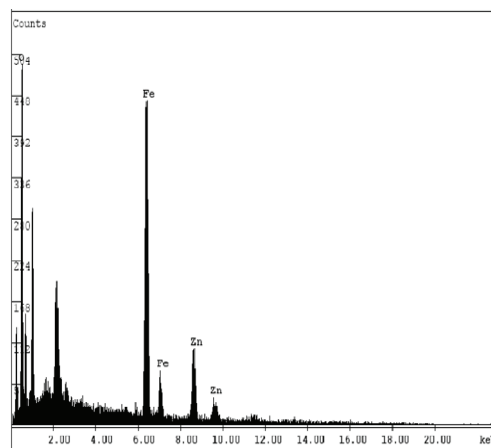


Figure 2. Energy Disperse X-ray Analysis spectrum of ZnFe_2O_4 nanocomposite.

SEM images of ZnFe_2O_4 nanocomposites are shown in Figure 3 (a) & (b). It can be observed that there is a non-uniform distribution of zinc ions in ferric oxide nanocomposites (before/after calcinations) with irregular shaped particles. It is evident that before calcination the samples have some agglomerates and are irregular in shape. After calcination a spherical in shape with uniform morphology can be seen and that there is a narrow size distribution of the particles.

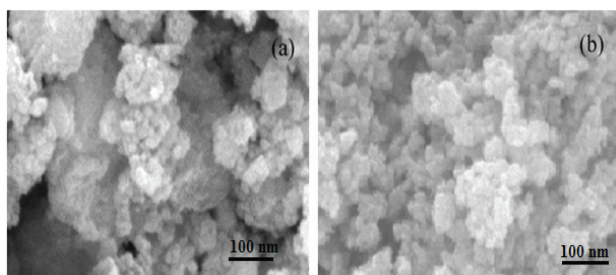


Figure 3. Scanning Electron Microscopy image of ZnFe_2O_4 nanocomposites (a) before calcination (b) after calcination.

Figure 4(a) presents a TEM observation of the ZnFe_2O_4 nanocomposites. The crystallite sizes were obtained from the analysis of TEM images and were in good agreement with the sizes determined by Debye-Scherrer approximation. Figure 4(b) shows a high resolution TEM image that indicates that the zinc ferrite's nanocomposites are highly porous in nature and the zinc particles are coagulated with ferrite particles. The average crystalline size was found to be 2nm.

5. Optical Properties

Metal nanoparticles have attracted much attention because of their distinctive electronic and optical properties arising from reduced dimensionality and a high surface-to-volume ratio. In accordance with this fact, absorption spectroscopy was used to monitor the polydispersity of nanoparticle sizes in a colloidal solution.

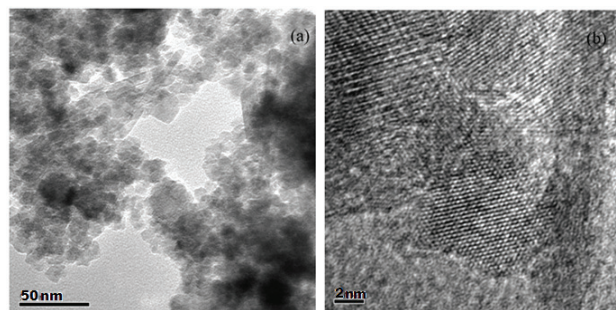


Figure 4. (a) Transmission electron microscopy micrograph and (b) High resolution transmission electron microscopy image of the same ZnFe_2O_4 nanocomposites.

The fluorescence spectra also provide fascinating information about the nanoparticles. The fluorescence

onset shifts with respect to the quantum confinement [14]. These results suggest that fluorescence spectroscopy is a useful tool for monitoring the nature of the nanoparticles' surface and how it changes with particle size.

It is exciting to note that there is a remarkable change in colour of ZnFe_2O_4 nanocomposites when dispersed in double distilled water and exposed to UV light. The experimental results exhibit a reddish brown colour at 450nm and an orange-red colour at 650nm, as shown in Figures 5(a) and 5(b).

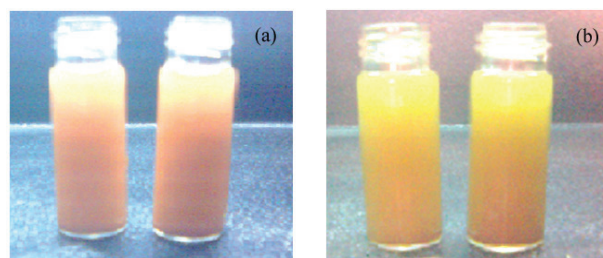


Figure 5. Change in colour when nanocomposites are dispersed in distilled water (a) 650nm (b) 450nm.

5.1 Absorption spectroscopy

The absorption spectra of ZnFe_2O_4 nanocomposites were recorded by dispersing the particles uniformly in the double distilled water in presence of HCl media (0.3N) at different concentrations (0.001, 0.002, 0.003, 0.004g/10ml) at a wavelength range of 250 to 800nm. ZnFe_2O_4 has been known to have strong absorption in the UV-Vis range [15, 16, 17]. As shown in Figure 6, the ZnFe_2O_4 nanocomposites have strong band edge absorption in the wavelength region of 250 to 800nm. The sharp absorption band formed at 334nm shows the overlap of optical property with the Beer-Lambert law. Figure 6 shows the variation of absorption with intensity at different concentrations and that the observed hyperchromic shift tends to be a small shift in electronic excitation. From the above results, it can be suggested that the prepared ZnFe_2O_4 nanocomposites are optically active.

5.2 Fluorescence properties

Figure 7 shows the room temperature fluorescence spectra (FL) of ZnFe_2O_4 nanocomposites with different concentrations, recorded in the 330 to 700nm wavelength range. Intense fluorescence emissions were observed under excitation at 367nm. In the entire FL spectrum, broad visible emission bands were observed. The first is the blue band at 367nm and the second is the orange-red band at 645nm. The blue emission at 376nm is attributed to the defect-related emission, particularly interstitial zinc defects [18].

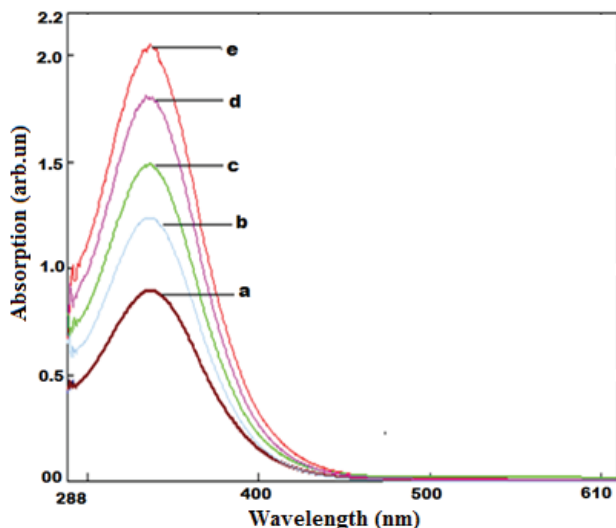


Figure 6. UV-Visible absorption spectra of ZnFe_2O_4 nanocomposites at different concentrations (a) 0.001g/10ml (b) 0.002 g/10ml (c) 0.003 g/10ml (d) 0.004 g/10ml (e) 0.005 g/10ml.

For the ZnFe_2O_4 nanocomposite samples, a second emission band in the yellow-orange region centred at about 647nm is observed, which is significantly contributed to by the Fe-Zn phase [19]. It can be observed that the sample gives out orange-yellow light, which corresponds to the FL spectrum result [16].

The highest intense peak corresponds to the maximum transition probability. If the wavelength of the radiation is λ and ΔE is the gap between the energy states, the transition probability is significant only when $h\nu = \Delta E$ or $hc/\Delta E$, in accordance with the Fermi golden rule [20]. Here the observed fluorescence emission spectra was widely varied depending upon the individual vibrational energy levels of the ground and excited states of ZnFe_2O_4 nanocomposites [21]. The fluorescent efficiency of ZnFe_2O_4 nanocomposites is estimated for different concentrations, as shown in Figure 7. As the concentration

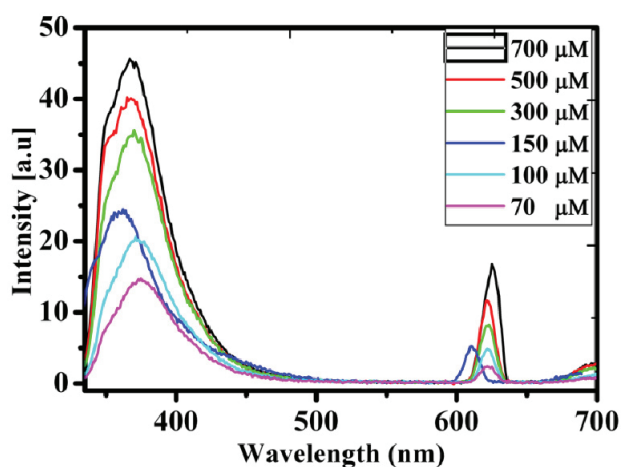


Figure 7. Room temperature fluorescence spectra of ZnFe_2O_4 nanocomposites with different concentrations.

of ZnFe_2O_4 nanocomposites was increased from $30\mu\text{M}$ to $700\mu\text{M}$, the corresponding intensities at 647nm were also amplified. An enhanced concentration of ZnFe_2O_4 nanocomposites led to a boost in the number of fluorescence centres, which contributed to the improvement in intensity as well as the electronic exchange within the ZnFe_2O_4 nanocomposites. Even with an increase in irradiation time, the intensity of the emission band positioned at about 647nm was enhanced and the trend was consistent with the changes in the corresponding surface plasmon band of these nanocomposites.

6. DC Electrical characterization

The obtained DC results reveal a variation in the electrical conductivity of the prepared samples with temperature (Figure 8). It was found that conductivity increases with an increase in temperature, showing a semiconducting behaviour. The two steps of conductivity are observed here: the first step in conductivity is almost constant with an increase in temperature of up to 490K, and in the second step, conductivity increases gradually beyond 490K. The graph of $\ln\sigma$ versus $1000/T$ (Figure 9) can be fitted into an Arrhenius plot, which has two straight lines with different slopes. This Arrhenius plot has a break at critical temperature $T_c = 490$ K, which is attributed to different conduction mechanisms.

The electrical conductivity in ferrites can be explained on the basis of exchange of electrons between ions of the same element that are present in more than one valence state distributed randomly over equivalent crystallographic lattice sites ($\text{Fe}^{3+} \leftrightarrow \text{Fe}^{2+}$) [22]. It is well known that the change in slope is attributed to the Curie temperature or to a change in the conduction mechanism [23-25]. At the Curie temperature, the samples transform from an ordered ferrimagnetic state to a disordered paramagnetic state with a marked increase in conductivity.

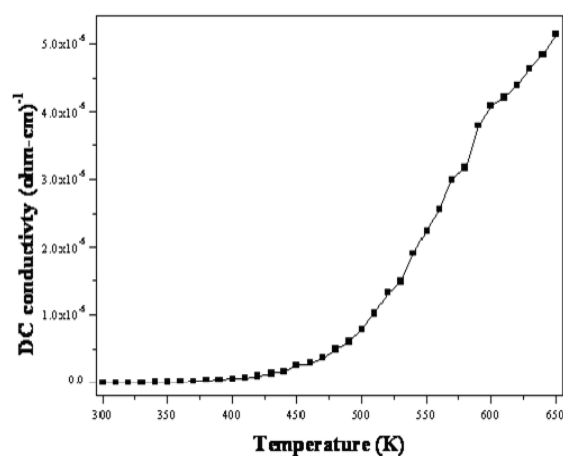


Figure 8. Variation of DC electrical conductivity with temperature.

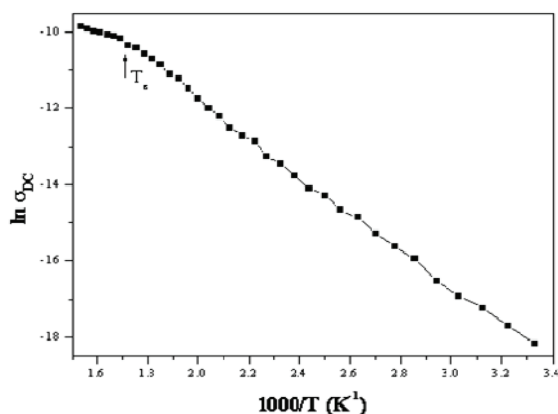


Figure 9. Arrhenius plot of ZnFe₂O₄ nanocomposites.

There are several results that reveal ferrimagnetic behaviour at room temperature [26]. Hence, the observed break at 490K may be due to a phase transition from ferrimagnetic to paramagnetic nature. The activation energies were different in these two regions and can be calculated from an Arrhenius plot near T_c. The calculated activation energy value in the ferrimagnetic and paramagnetic regions were found to be 0.49eV and 0.55eV, respectively. In the ferrimagnetic region, the conductivity is due to electron hopping between Fe²⁺ and Fe³⁺ ions in B sites, which results in a lower value of activation energy. In the paramagnetic region a higher value of activation energy was found, which suggests that the conduction mechanism in this temperature range is different from that of low temperature region. The prepared sample was calcined at 400K, during that time the oxygen ions escape from the spinel structure and thereby create anion vacancies. Therefore, the conduction due to anion vacancies may be responsible for the increase in conductivity due to the higher activation energy in the high temperature region.

7. Conclusion

The ZnFe₂O₄ nanocomposites were prepared by employing a co-precipitation method. The XRD confirms that the highest intensity peaks were at 2θ=34.87°, which corresponds to the reflection plane (311) and the average particle size was found to be 20±5nm. SEM results reveal that before calcinations samples have some agglomerates and are irregular in shape but after calcination samples show uniform and almost spherical structural morphology with a narrow size distribution of particles. The changes observed in fluorescence emission spectra at the range of 550nm-70 nm of ZnFe₂O₄ nanocomposites were due to the oscillation of electrons from a ground state to an excited state. Finally, the electrical conductivity of the nanocomposites increases with increase in temperature, which is the observed behaviour of semiconductor materials. It is also observed that, the ZnFe₂O₄ nanocomposites undergo a transition from a ferrimagnetic state to a paramagnetic state.

8. Acknowledgements

The author would like to thank UGC for providing the Rajiv Gandhi National Fellowship (JRF). The author acknowledges IISc, Bangalore for providing spectral data.

9. Reference

- [1] M. Bruchez, M. Moronne Jr., P. Gin, S. Weiss, A. Paul, "Semiconductor nanocrystals as fluorescent biological labels", *Alivisatos Science*, New Series, vol. 281, pp. 2013-2016, 1998.
- [2] C. Degueldre, G. Kuri, C.N. Borca, D. Grolimund "X-ray micro- fluorescence, diffraction and absorption spectroscopy for local structure investigation of a radioactive zinc ferrite deposit" *Journal of Corrosion Science*, vol. 51, pp.1690-1695, 2009.
- [3] K. Aslan, M. Wu, R. Joseph, L. D. Chris, Geddes, "Fluorescent Core-Shell Ag@SiO₂ Nanocomposites for Metal Enhanced Fluorescence and Single Nanoparticle Sensing Platforms", *J. Am. Chem. Soc.*, vol. 129, pp. 1524-1525, 2007.
- [4] A.D. Schwartz, S. Nick, Norberg, P.Q. Nguyen, M. J. Parker, R.D. Gamelin, "Magnetic Quantum Dots: Synthesis, Spectroscopy, and Magnetism of Co²⁺- and Ni²⁺-Doped ZnO Nanocrystals", *J. Am. Chem. Soc.*, vol. 125, pp. 13205-13218, 2003.
- [5] X. Hong, J. Li, M. Wang, J. Xu, W. Guo, J. Li, Y. Bai, T. Li, "Fabrication of Magnetic Luminescent Nanocomposites by a Layer-by-Layer Self-assembly Approach", *Chem. Mater.*, vol. 16, pp. 4022-4027, 2004.
- [6] H. S. Qian, Y. Hu, Z. Q. Li, X. Y. Yang, L.C. Li, X. T. Zhang, and R. Xu "ZnO/ZnFe₂O₄ Magnetic Fluorescent Bifunctional Hollow Nanospheres: Synthesis, Characterization, and Their Optical/Magnetic Properties" *J. Phys. Chem. C*, vol. 114, pp.17455-17459, 2010.
- [7] N. Ponpandian, A. Narayanasamy, C. N. Chinnasamy, N. Sivakumar, J.M. Greneche, K. Chattopadhyay, K. Shinoda, B. Jeyadevan, K. Tohji, "Néel temperature enhancement in nanostructured nickel zinc ferrite", *Applied Physics Letter*, vol. 86, pp. 192510-192512, 2005.
- [8] D.J. Norris, N. Yao, F.T. Charnock, T.A. Kennedy, "High-Quality Manganese-Doped ZnSe Nanocrystals", *Nano Lett.*, vol. 1, pp. 3-7, 2001.
- [9] N. Guskos, S. Glenis, G. Zolnierkiewicz, J. Typek, P. Berczynski, A. Guskos, D. Sibera, and U. Narkiewicz, "Magnetic properties of ZnFe₂O₄ ferrite nanoparticles embedded in ZnO matrix" *Applied Physics Letters*, vol. 100, pp. 122403, 2012.
- [10] H.R. Prakash Naik, H.S. Bhojya Naik, G.S. Yashavanth Kumar, "TiO₂ Nanoparticles: Synthesis and Evaluation of In Vitro Antioxidant Activity", *Nano Trends. A Journal of Nanotechnology and its Applications*, vol. 8, pp. 28, 2010.

- [11] H. Kim, M. Achermann, P. Laurent Balet, A. Jennifer Hollingsworth, I. Victor Klimov, "Synthesis and Characterization of Co/CdSe Core/Shell Nanocomposites: Bifunctional Magnetic-Optical Nanocrystals", *J. Am. Chem. Soc.* vol. 127, pp. 544-546, 2005.
- [12] B. P. Rao, A.M. Kumar, K.H. Rao, Y.L. N. Murthya, O.F. Caltunb, I. Dumitru, I. Spinuc, "Synthesis and magnetic studies of Ni-Zn ferrite nanoparticles", *Journal Of Optoelectronics And Advanced Materials*, vol. 8, pp. 1703-1705, 2006.
- [13] B. D. Cullity, "Elements of X-ray Diffraction", *Adison-Wesley Publ. Co., London*. 1967. M. Kasha, "Characterization of electronic transitions in complex molecules", *Disc faraday Soc.*, vol. 9, pp. 14-19, 1950.
- [14] F. C. Landes, M. Braun, A. M. El-Sayed. "On the Nanoparticle to Molecular Size Transition: Fluorescence Quenching Studies", *J. Phys. Chem. B.*, vol. 105, pp. 10554-10558, 2001.
- [15] Z.H. Yuan, W. You, J.H. Jia, L.D. Zhang, "Optical Absorption Red Shift of Capped ZnFe₂O₄ Nanoparticle", *Chin. Phys. Lett.*, vol. 15, pp. 535-536, 1998.
- [16] Z. Wu, M. Okuya, S. Kaneko, "Spray pyrolysis deposition of zinc ferrite films from metal nitrates solutions", *Thin Solid Films*, vol. 385, pp. 109-114, 2001
- [17] E. Marquez, J. R. Malo, P. Villares, R. J. Garay, P.J.S. Ewen, A.E. Owen, "Calculation of the thickness and optical constants of amorphous arsenic sulphide films from their transmission spectra", *J. Phys. D Appl. Phys.*, vol. 25, 535-541, 1992
- [18] A. K. Srivastava, M. Deepa, N. Bahadur, M.S. Goyat, "Influence of Fe doping on nanostructures and photoluminescence of sol-gel derived Zn", *Mater. Chem. Phys.*, vol. 114, pp. 194-198, 2009
- [19] A.J. Chen, X.M. Wu, Z.D. Sha, L.J. Zhuge, Y.D. Meng, "Structure and photoluminescence properties of Fe-doped ZnO thin films", *J. Phys. D Appl. Phys.*, vol. 39, 4762-4765, 2006
- [20] A. K. Ghatak, S. Loknathan, "Quantum Mechanics, Theory and Applications", *Macmillan India Ltd, India*, pp. 503, 1984.
- [21] O. P. Siwach, P. Sen, "Synthesis and study of fluorescence properties of Cu nanoparticles", *J Nanopart Res.*, vol. 10, 107-114, 2008.
- [22] B.R. Karche, B.V. Khasbardar, A.S. Vaingankar, "X-ray, SEM and magnetic properties of Mg-Cd ferrites", *Journal of Magnetism and Magnetic Materials*, vol. 168, pp. 292-298, 1997.
- [23] J. M. Song, J.G. Koh, "Studies on the electrical properties of polycrystalline cobalt-substituted lithium ferrites", *Journal of Magnetism and Magnetic Materials*, vol. 152, pp. 383-386, 1996.
- [24] A. A. Sattar, "Temperature Dependence of the Electrical Resistivity and Thermoelectric Power of Rare Earth Substituted Cu - Cd ferrite", *Egypt. J. Sol.*, vol. 26, pp. 113-121, 2003.
- [25] D. Ravinder, T. S. Rao, "Electrical conductivity and thermoelectric power of lithium-cadmium ferrites", *Crystal Research and Technology*, vol. 25, pp. 963-969, 1990.
- [26] C. N. Chinnasamy, A. Narayanasamy, N. Ponpandian, "Magnetic properties of nanostructured ferrimagnetic zinc ferrite", *J. Phys.: Condens. Matter*, vol. 12, pp. 7795-7805, 2000.